Chemical Science

ROYAL SOCIETY OF CHEMISTRY

EDGE ARTICLE

View Article Online
View Journal | View Issue

Cite this: *Chem. Sci.*, 2024, **15**, 20448

All publication charges for this article have been paid for by the Royal Society of Chemistry

Received 9th September 2024
Accepted 8th November 2024

DOI: 10.1039/d4sc06109h

rsc.li/chemical-science

Ligand cross-links as a design element in oligo- and polyMOFs†

Debobroto Sensharma and Seth M. Cohen *

Metal–Organic Frameworks (MOFs) constructed using cross-linked oligomeric or polymeric ligands (oligoMOFs and polyMOFs respectively) have so far relied on a handful of canonical structural blueprints, in which the cross-links have not played a significant role in determining structure. In this study, we show that cross-links between terephthalate ligands in dabco-based Zn-MOFs (DMOFs) can exert control over the overall phase landscape of resulting oligo- and polyMOFs. We find that cross-links can direct the overall topology of the resulting MOF (**pcu** *vs.* **kag**) based on their length or rigidity, and can influence the phase transformation behavior of the **pcu** network. We also show the first example of tethered ligand dimers adopting a different MOF structure to the analogous trimer and polymer. Understanding the influence of cross-links on the formation of these MOFs will help guide the design of future MOF–polymer hybrid materials.

Introduction

The modular nature of metal–organic frameworks (MOFs) has been one of the main motivations behind the broad research interest in this class of solids in the past several decades.[1–5] MOFs can be constructed with predetermined architectures by judiciously selecting molecular building blocks, *i.e.*, organic ligands and metal atoms or clusters of appropriate geometries. This approach, known as reticular chemistry, has been demonstrated powerfully by the construction of large families of isoreticular MOFs in which a single building block is substituted by others of the same connectivity and geometry, ultimately resulting in structures that share the same network topology, but show predictable differences in pore size and functionality.[6–9] However, in some cases, MOFs adopt different network topologies even though they are constructed using identical molecular building blocks. This phenomenon is known as framework isomerism[10–12] and is exemplified by groups of MOFs such as **MIL-101** (**mtn** network) and **MIL-88B** (**acs** network),[13,14] **UiO-66** (**fcu**) and **EHU-30** (**hex**),[15] and **MOF-177-*m*NH$_2$** (**qom**), **MOF-155** (**pyr**), and **MOF-156** (**rtl**).[16]

Typically, distinct framework isomers are favored under different crystallization conditions, and these differences are utilized in synthesizing phase pure isomeric frameworks. In the case of the **pcu** and **kag** framework isomers of the archetypal "pillar-layered" MOF, **DMOF-1**, the **kag** structure is favored under kinetically controlled conditions, while the **pcu** structure is favored under thermodynamically forcing conditions. Following the discovery of each phase by Kim *et al.* and Chun *et al.*,[17,18] work by Kitagawa *et al.* has shown that the formation of the triangular structural subunits of the **kag** network is initially favored by the constituent Zn(II) paddlewheels and terephthalate (bdc^{2-}) ligands over the **pcu** network due to steric considerations (Fig. 1(a–d)).[19] Under kinetically controlled conditions, these triangular subunits act as nuclei for the growth of the **kag** framework. However, the extended **pcu** structure is energetically favored over **kag**, and is obtained upon the provision of sufficient thermal energy and reaction time. These differences were utilized by the groups of Verpoort and Walton to develop a rapid room temperature synthetic route to **kag-DMOF-1**, while also observing that the use of certain solvents instead favored the formation of **pcu-DMOF-1** under the same conditions.[20,21] Additionally, Verpoort *et al.* have shown that solvents such as MeOH can mediate the transformation of **kag-DMOF-1** to the thermodynamically favored **pcu-DMOF-1** by simply soaking in the solvent at room temperature.[22] Besides these isomeric structures, **DMOF-1** also exhibits distinct phases of the **pcu** isomer through flexibility. These phases involve distortions of the framework induced by interactions with various guest molecules such as DMF, benzene, and isopropanol. The relationships between these phases and topologies is summarized in Fig. 1(e).

Numerous studies have explored the effect of introducing substituent groups to the terephthalic acid linker in **DMOF** analogues, especially with respect to modulation of the adsorption-induced phase change behavior of the resulting frameworks.[23–30] However, despite the variety of functional variants that have been made, the introduction of additional

Department of Chemistry and Biochemistry, University of California San Diego, La Jolla, California 92093, USA. E-mail: scohen@ucsd.edu

† Electronic supplementary information (ESI) available: General experimental details, synthetic procedures for all ligands and MOFs, adsorption data, Pawley refinement data, ^{1}H digestion NMR data, Fig. S1–S60, and Tables S1–S4. See DOI: https://doi.org/10.1039/d4sc06109h

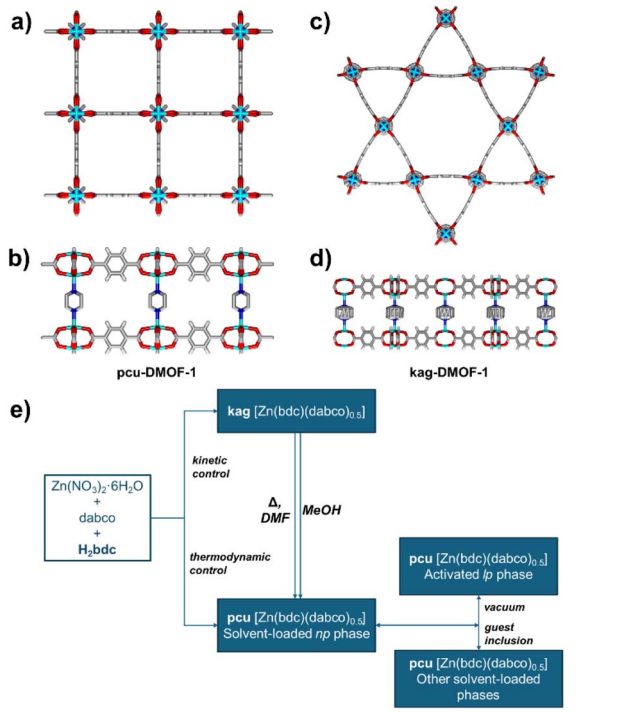

Fig. 1 Crystal structures of (a and b) **pcu-DMOF-1** and (c and d) **kag-DMOF-1**; (e) schematic representation of the phases of **DMOF-1** upon use of different synthetic conditions or other stimuli.

substituents to the H_2bdc linker has not been reported to yield the **kag** structure, which Hungerford and Walton attribute to steric constraints.[21]

Recent work from the laboratories of Xiao, Johnson, He, Zhou, Cohen, and others, has explored the outcomes of incorporating flexible tethering groups between conventional ligands, resulting in oligomeric (oligoMOF) or polymeric (polyMOF) materials.[31–42] These tethers are sufficiently flexible to allow the retention of the overall network structure of the analogous untethered "parent" MOF, but can, in principle, impose constraints on the relative distance and orientation between the tethered bdc^{2-} ligands. OligoMOF analogues of materials like **IRMOF-1** (**MOF-5**), **NOTT-101**, and **MOF-74** have been synthesized using this approach, which show modified properties owing to the incorporation of the tethering alkyl chains, such as modified sorbate uptake or exploitable surface functionality.[31,32,41,43] Notably, Xiao *et al.* showed that tether incorporation in an expanded **MIL-53** analogue could modulate its phase change behavior. The tether stabilized the large-pore phase of the material, which is unfavored at low guest loadings in the untethered "parent" MOF.[37]

The use of ligands linked into polymers through repeating cross-links in a similar manner yields polyMOFs, which also typically adopt canonical MOF structures. Studies on systems such as **IRMOF-1** and **UiO-66** emphasize the versatility of these systems with respect to the polymer chains incorporated, without altering the overall crystalline lattice.[31,32,44] In the examples reported so far, dimeric, trimeric, and polymeric tethers have adopted the same framework structure when combined with metal precursors under fixed conditions, and the number of repeating units has not been a factor in determining the structure adopted.

Despite some indications in previous studies that tether incorporation can result in unidentified phases, and that tether length can influence framework ordering relative to a single parent structure, the potential of tethers to influence the selection of competing structures has not been studied yet. In this work, we study the effects of joining terephthalic acid linkers with flexible alkyl chains and rigid xylyl spacers, in place of unmodified terephthalic acid in the synthesis of **DMOF-1**. We also study the impact of changing the number of repeating units on structure selection. The observed effect of ligand cross-linking on topology selection and phase transformations shows that flexible tethers may act as hitherto unstudied crystal engineering elements in the design and synthesis of MOFs, opening up a new chemical space for MOF discovery.

Results and discussion

Tethered oligomeric and polymeric H_2bdc ligands were prepared according to reported procedures (see ESI†). These ligands feature H_2bdc groups tethered using ether linkages by flexible *n*-alkyl chains of varying length, **butyl(bdc)$_2$**, **pentyl(bdc)$_2$**, **hexyl(bdc)$_2$**, and **heptyl(bdc)$_2$**; relatively rigid xylyl groups with similar numbers of carbon atoms between ether oxygens: ***o*-xylyl(bdc)$_2$**, ***m*-xylyl(bdc)$_2$**, and ***p*-xylyl(bdc)$_2$**; a trimeric linker, **pentyl$_2$(bdc)$_3$**; and polymeric linkers with *n*-pentyl and *n*-heptyl spacers: **pbdc-5a** and **pbdc-7a** (Fig. 2). We use the above terms to refer to cross-linked ligands in both protonated and fully deprotonated states. Polymer formation in the cases of **pbdc-5a** and **pbdc-7a** was confirmed by MALDI-TOF MS (Fig. S1 and S2†). Oligomeric ligands were combined with zinc nitrate hexahydrate and 1,4-diazabicyclo[2.2.2]octane (dabco) in DMF and heated under solvothermal conditions using a procedure optimized for the synthesis of the parent **pcu-DMOF-1** (ESI†). Previously reported synthetic difficulties associated with the synthesis of polyDMOFs were overcome by

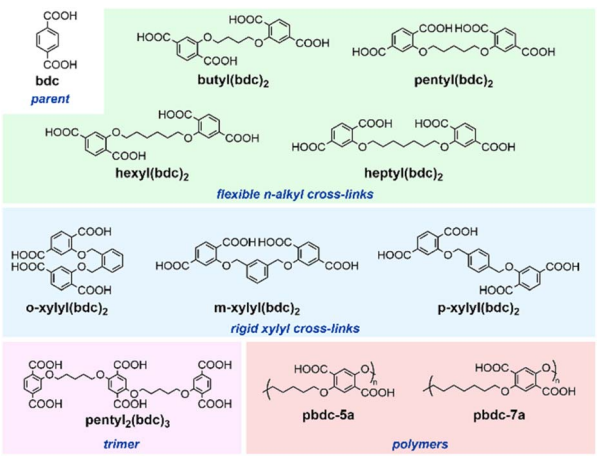

Fig. 2 The cross-linked terephthalic acid ligands chosen for the construction of oligo- and poly-DMOFs.

modifying the synthetic procedure, allowing a precipitate to form upon mixing reactants, and subjecting the suspension to solvothermal conditions without filtering the solids out.[45] The parent **kag-DMOF-1** was synthesized using the "rapid" procedure reported by Hungerford and Walton.[21] In order to keep the proportion of Zn^{2+}, dabco, and bdc^{2-} units identical across reactions with various tethered ligands, the number of moles of dimeric ligands (which contain two H_2bdc units per formula mass) was halved relative to the procedure using untethered H_2bdc, and the number of moles of pentyl$_2$(bdc)$_3$ was reduced by a factor of three. The number of moles of polymer ligands was not changed, since they contain one bdc unit per formula unit.

Polycrystalline products were obtained from these reactions and were characterized by powder X-ray diffraction (PXRD), N_2 physisorption (at 77 K), and ^{1}H NMR (after digestion of the solid in acid). Upon comparison of the PXRD patterns obtained from the alkyl-tethered DMOFs, we find that although these reactions were carried out under identical conditions, the crystal structures adopted are clearly distinct (Fig. 3). The patterns shown by **butyl(bdc)$_2$-DMOF-1** and **pentyl(bdc)$_2$-DMOF-1** closely match the calculated pattern for **kag-DMOF-1** with a characteristic 2θ peak at *ca.* 4.7°, whereas that shown by **heptyl(bdc)$_2$-DMOF-1** matches the calculated pattern for **pcu-DMOF-1**, with a characteristic 2θ peak at *ca.* 8.1°. The adoption of a phase pure **kag** structure by **butyl(bdc)$_2$-DMOF-1** and **pentyl(bdc)$_2$-DMOF-1**, under conditions that yield the phase pure **pcu** structure using unfunctionalized terephthalic acid implies that the butyl and pentyl cross-links direct the adoption of the **kag** structure. This shows that the formation of the **kag** structure using functionalized bdc^{2-} units is possible, but more importantly, that the cross-link between bdc^{2-} units exerts a structure-directing influence under conditions that typically result in the **pcu** structure. The PXRD pattern of the putative **hexyl(bdc)$_2$-DMOF-1** does not correspond to either of these phases. The possibility of additional phases in the DMOF system was noted by Kitagawa *et al.* in their study of framework isomerism in **DMOF-1**, and this material too may represent a novel structural arrangement.[19]

PXRD patterns obtained for ***o*-xylyl(bdc)$_2$-DMOF-1**, ***m*-xylyl(bdc)$_2$-DMOF-1**, and ***p*-xylyl(bdc)$_2$-DMOF-1** all match the calculated **pcu-DMOF-1** pattern (Fig. 4). This is notable because of the similarity in the number of carbon atoms between ether oxygens in each linker: four in ***o*-xylyl(bdc)$_2$** and **butyl(bdc)$_2$**, five in ***m*-xylyl(bdc)$_2$** and **pentyl(bdc)$_2$**, and six in ***p*-xylyl(bdc)$_2$** and **hexyl(bdc)$_2$**. None of the flexible alkyl-tethered linkers of corresponding lengths yielded **pcu** structures, implying that the rigidity of the xylyl tethers impose geometrical constraints incompatible with the formation of the **kag** structure.

The trimer-based **pentyl$_2$(bdc)$_3$-DMOF-1** and polymeric **pbdc-5a-DMOF-1** also adopted the **pcu** structure, in contrast to the dimeric **pentyl(bdc)$_2$-DMOF-1** based on the same spacer (Fig. 5). This is the first observation of corresponding dimeric and trimeric oligoMOFs adopting distinct, isomeric framework structures, as well as the first example of isomerism between the framework structures of an oligoMOF and its exact polyMOF analogue. These results show the remarkable sensitivity of the **DMOF** system to subtle changes in the length, flexibility, and number of repeat units of tethered H_2bdc ligands. Despite facile data collection on a laboratory source, Pawley refinement of the PXRD patterns of these MOFs showed good whole pattern fits, high phase purity, and minimal deviation of unit cell parameters from the reported single crystal structures of the parent **pcu-DMOF-1** and **kag-DMOF-1** (Table S1 and Fig. S3–S11†).

To better understand the role of the alkyl cross-link in directing the formation of isomeric networks, we conducted further experiments on **pentyl(bdc)$_2$-DMOF-1** and **heptyl(bdc)$_2$-DMOF-1**. When synthetic conditions were changed to the rapid method outlined by Hungerford and Walton, in which unfunctionalized terephthalate forms the **kag** network in the presence of triethylamine and DMF (see ESI Fig. S12†), the PXRD pattern of the product formed using **pentyl(bdc)$_2$** is well-

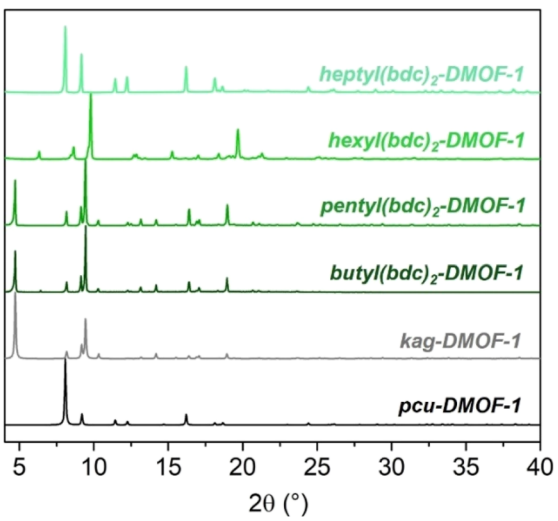

Fig. 3 PXRD patterns of alkyl-tethered DMOFs in comparison with pcu-DMOF-1 and kag-DMOF-1.

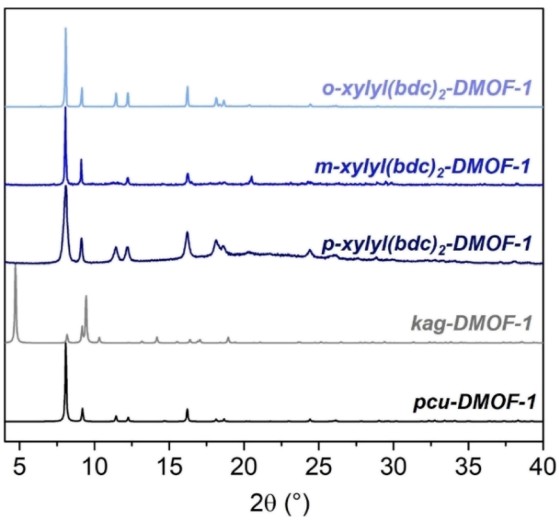

Fig. 4 PXRD patterns of xylyl-tethered DMOFs in comparison with pcu-DMOF-1 and kag-DMOF-1.

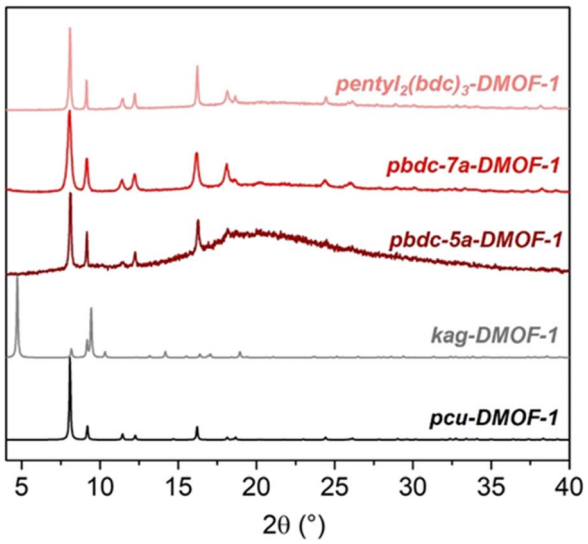

Fig. 5 PXRD patterns of trimer- and polymer-based DMOFs in comparison with **pcu-DMOF-1** and **kag-DMOF-1**.

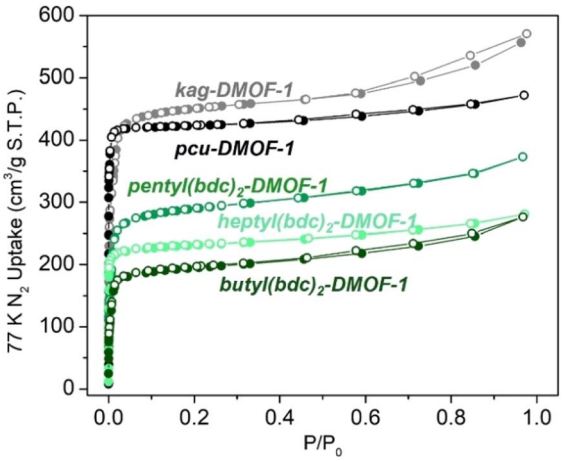

Fig. 6 N_2 sorption isotherms (77 K) of alkyl-tethered DMOFs in comparison with **pcu-DMOF-1** and **kag-DMOF-1**. Closed symbols represent adsorption and open symbols represent desorption.

defined and corresponds to the phase pure **kag** product. However, under the same conditions, the **heptyl(bdc)$_2$** product shows poor crystallinity, only retaining the major peaks associated with the **pcu** structure. Therefore, although conditions that promote the formation of the kinetically favored **kag** structure do influence the reaction, the effect of the pentyl and heptyl cross-links remains the same as under solvothermal conditions. In addition, this observation shows that the heptyl cross-link also exerts its own structure directing effect on the product.

To investigate whether the pentyl cross-link permits the formation of the **pcu** structure under thermodynamically forcing conditions, we allowed solvothermal syntheses using **pentyl(bdc)$_2$** to proceed for up to two weeks. PXRD patterns taken after one week and two weeks under these conditions showed the exclusive formation of the **kag** phase of **pentyl(bdc)$_2$-DMOF-1** with no discernible decrease of crystallinity, suggesting that the modulation of the landscape of available structures by the pentyl cross-link is indeed of a thermodynamic nature (Fig. S13†). This is consistent with observations from solvent soaking experiments, in which we observe that **pentyl(bdc)$_2$-DMOF-1** shows no change from its **kag** structure or decrease in crystallinity upon soaking for up to a week in solvents including MeOH, whereas unfunctionalized **kag-DMOF-1** transforms to the **pcu** isomer in less than 72 hours under the same conditions, in agreement with Verpoort *et al.* (Fig. S14†).[22]

N_2 physisorption experiments carried out on the tethered DMOFs showed the retention of appreciable BET surface areas in most materials, with characteristic Type I isotherms. Among alkyl-tethered DMOFs, BET surface area values varied from 841 ± 60 and 1150 ± 4 m^2 g^{-1} for **butyl(bdc)$_2$-DMOF-1** and **pentyl(bdc)$_2$-DMOF-1**, respectively to 962 ± 1 m^2 g^{-1} for **heptyl(bdc)$_2$-DMOF-1** (Fig. 6). These values are reduced relative to the values obtained for the parent **pcu-DMOF-1** and **kag-DMOF-1**, 1779 ± 58 m^2 g^{-1} and 1813 ± 22 m^2 g^{-1}, due to partial occlusion of pores by the flexible tethering moieties. Pore volumes were found to be 0.429 cm^3 g^{-1} and 0.578 cm^3 g^{-1} for butyl and pentyl tethered **kag** DMOFs, compared to 0.863 cm^3 g^{-1} in the parent **kag-DMOF-1**. The pore volume of **heptyl(bdc)-DMOF-1** was found to be 0.443 cm^3 g^{-1}, compared to 0.732 cm^3 g^{-1} in **pcu-DMOF-1**. These values confirm that large fractions of the parent pore volume are retained in oligo-DMOFs adopting both **kag** and **pcu** structures, despite the incorporation of tethering groups.

MOFs constructed using the xylyl-tethered H_2bdc linkers showed BET surface areas of 1093 ± 84 m^2 g^{-1} for ***o*-xylyl(bdc)$_2$-DMOF-1**, 892 ± 1 m^2 g^{-1} for ***m*-xylyl(bdc)$_2$-DMOF-1**, and 892 ± 1 m^2 g^{-1} for ***p*-xylyl(bdc)$_2$-DMOF-1** (Fig. S15†). These three MOFs adopt the **pcu** structure, and the surface area available varies systematically with the increased centrality of the bulky phenyl ring in the tethered ligand molecule. This trend is also observed in pore volumes. The trimer-based **pentyl$_2$(bdc)$_3$-DMOF-1** shows reduced porosity compared to its parent or dimer-based counterparts, and has a BET surface area of 448 ± 88 m^2 g^{-1}. The pentyl-spaced polyMOF, **pbdc-5a-DMOF-1** shows minimal microporosity with a BET surface area of just 100 ± 6 m^2 g^{-1}. The heptyl-spaced polyMOF, **pbdc-7a-DMOF-1**, retains more of its microporosity in comparison, with a BET surface area of 251 ± 5 m^2 g^{-1} (Fig. S16†). The reduced porosity observed in polyDMOFs compared to oligoDMOFs is consistent with the increased density of tethering units in polyDMOFs – 1 tethering unit per bdc unit in polymeric linkers, *versus* 0.5 tethering unit per bdc unit in dimer linkers – resulting in greatly diminished accessible void space in the ultramicroporous MOF structure.

The observation of varying degrees of crystallinity between oligo- and polyDMOFs bearing different tethering groups is found to correlate with the observation of varying degrees of macropore N_2 condensation in the high-pressure region of the respective isotherms. Materials with less crystalline PXRD patterns, such as ***p*-xylyl(bdc)$_2$-DMOF-1**, **pentyl$_2$(bdc)$_3$-DMOF-1**, **pbdc-5a-DMOF-1**, and **pbdc-7a-DMOF-1**, show noticeably larger

steps due to macropore condensation, suggesting a relationship between crystal attributes such as size, morphology, defectivity, and N_2 uptake.

Pore size distributions calculated from these isotherms by the Horvath–Kawazoe (HK) method provided corroborating structural insights (Table S2†). The parent **pcu-DMOF-1** shows a sharp unimodal distribution of pore widths with a maximum at *ca.* 6.1 Å, whereas the parent **kag-DMOF-1** shows a bimodal distribution of pore widths due to the presence of narrow triangular (*ca.* 6.3 Å) and broad hexagonal (*ca.* 11.3 Å) microporous channels (Fig. S17–S27†). We observe that tethered DMOFs adopting the **kag** structure, **butyl(bdc)$_2$-DMOF-1** and **pentyl(bdc)$_2$-DMOF-1**, also show bimodal pore size distributions, while those that adopt the **pcu** structure show unimodal distributions. In contrast to the small deviations from the parent structures found in unit cell parameters, deviations from the pore size distribution maxima in the tethered material were found to be as large as *ca.* 1.0 Å. Pore contraction due to the incorporation of tethering groups can account for many of these deviations, but in some cases, such as the increase of the HK plot maximum associated with the micropore in ***o*-xylyl(bdc)$_2$-DMOF-1** and ***p*-xylyl(bdc)$_2$-DMOF-1**, and the triangular micropore in **butyl(bdc)$_2$-DMOF-1** and **pentyl(bdc)$_2$-DMOF-1**, distortion of framework components (*e.g.* torsion of phenyl rings) is suggested.

^{1}H NMR experiments carried out on activated and acid-digested MOFs confirmed that cross-links in each ligand were intact and provided information on the composition of each material, by integration of proton signals corresponding to tethered H_2bdc ligands and the single peak corresponding to dabco (Table S3 and Fig. S28–S39†). This method confirms that the parent MOFs show a H_2bdc-to-dabco mole ratio of 2 : 1, corresponding to the expected formula of $[Zn_2(bdc)_2(dabco)]$. The dimeric oligoDMOFs in this study conform to a general formula of $[Zn_2(tether(bdc)_2)(dabco)]$, and the trimer-based **pentyl$_2$(bdc)$_3$-DMOF-1** conforms to a formula of $[Zn_3(pentyl_2(bdc)_3)(dabco)_{1.5}]$. The polyDMOFs have an expected H_2bdc-to-dabco mole ratio of 2 : 1. However while **pbdc-7a-DMOF-1** agrees with this ratio, the ratio found for **pbdc-5a-DMOF-1** is nearly 3 : 1. Since ^{1}H NMR conducted on thoroughly washed but unactivated **pbdc-5a-DMOF-1** (Fig. S40†) shows the expected H_2bdc-to-dabco mole ratio of 2 : 1, the loss of dabco linkers can be attributed to degradation of the framework structure during activation. Finally, ^{1}H NMR of the as-synthesized **hexyl(bdc)$_2$-DMOF-1** material indeed conformed to the expected bdc : dabco mole ratio of 2 : 1, and may indicate a novel framework isomer of **DMOF**. Work to prepare single crystalline samples of **hexyl(bdc)$_2$-DMOF** is ongoing.

FTIR spectra of the activated oligoDMOFs (Fig. S41–S49†) do not show any observable peaks in the region between 1720 cm^{-1} and 1680 cm^{-1}, which is associated with the C=O stretching vibration (ν_s C=O) of the free carboxylate groups in the respective tethered ligands. Instead, strong peaks associated with the asymmetric –COO$^-$ stretching mode (ν_{as} COO$^-$) of coordinated carboxylates are observed in each case between 1640 cm^{-1} and 1630 cm^{-1}. This implies that uncoordinated carboxylate groups are not present in the oligo-MOFs in significant quantities. However, small shoulders are observed at *ca.* 1720 cm^{-1} in the FTIR spectra of the polyDMOFs (Fig. S48 and S49†), suggesting that although the peak intensity and area corresponding to the ν_s C=O stretch are greatly reduced, a notable fraction of carboxylate groups remain uncoordinated unlike in the oligoDMOFs, and that the additional constraints imposed by multiple repeating units hinder the efficient binding of all carboxylate groups in the **pcu** structure.

Examination of PXRD patterns of these materials before and after activation (Fig. 7) shows that the dimeric oligoDMOFs adopting **pcu** networks do not show noticeable structural changes upon activation, unlike **pcu-DMOF-1** which is known to undergo a phase transformation. Although cross-linked DMOFs adopt a **pcu** network, the incorporation of the heptyl cross-link results in clear phase differences from unfunctionalized **DMOF-1**. Whereas the flexibility of **DMOF-1** results in the adoption of a narrow pore DMF-loaded phase upon solvothermal synthesis, the structures of as synthesized **heptyl(bdc)$_2$-DMOF-1** and **pbdc-7a-DMOF-1** closely resemble the large pore phase that corresponds to the guest-free **DMOF-1** structure.[17] This difference between phases is illustrated by a shift of the (100) peak from 8.25° (2θ) in the narrow pore phase to 8.10° (2θ) in the large pore phase.

Xylyl-tethered oligoDMOFs, **pentyl$_2$(bdc)$_3$-DMOF-1**, and **pbdc-5a-DMOF-1** which all adopt **pcu** networks similarly form the large pore phase directly upon synthesis in DMF. The assignment of phases in this manner is corroborated by Pawley refinement of PXRD data for all **pcu** oligoDMOFs against the large pore parent **pcu-DMOF-1** structure. We postulate this is due to the occupation of a large fraction of the pore volume of the structure by the cross-links, which may act as *de facto* guests and prevent pore contraction. Therefore, cross-links effectively "lock" each **pcu** structure into its large pore phase (Fig. S50†). To our knowledge, this is the second case of large pore phase stabilization upon cross-link incorporation, following the report

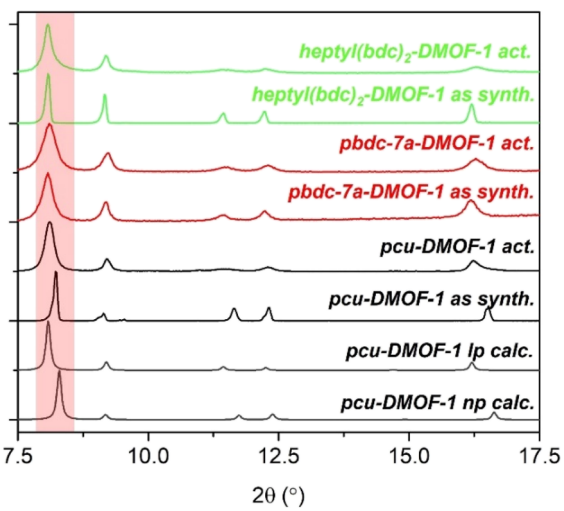

Fig. 7 PXRD patterns of as synthesized and activated DMOFs in comparison with **pcu-DMOF-1**. The red region highlights the (100) peak.

by Xiao *et al.*[37] However, the **pcu** structures obtained using pentyl cross-links, **pentyl$_2$(bdc)$_3$-DMOF-1** and **pbdc-5a-DMOF-1**, do show significant losses in crystallinity upon solvent removal at elevated temperature. This, taken together with the dabco linker vacancies seen in the NMR spectrum of digested **pbdc-5a-DMOF-1**, indicates that although increasing the number of repeating H_2bdc units to three or greater directs the formation of **pcu** structures, these structures may be more strained and less robust than other **pcu** oligo- or polyDMOFs with better matches in cross-link length and framework dimensions.

Further insight into the stability of these materials is obtained from thermogravimetric analysis (TGA). After showing initial mass loss due to vaporization of interparticle and pore DMF below 200 °C, the **kag** oligoDMOFs based on butyl and pentyl cross-links show mass loss steps due to decomposition, with onsets at approximately 310 °C and 305 °C respectively, close to the reported value of 300 °C for the parent **kag-DMOF-1** (Fig. S51 and S52†). Similarly, heptyl and xylyl-tethered **pcu** oligoDMOFs show decomposition steps between 325 °C and 335 °C, in agreement with reported values for **pcu-DMOF-1** (Fig. S53–S56†). However, while **pbdc-7a-DMOF-1** shows a similar decomposition temperature to the **pcu** oligo-DMOFs (325 °C), **pentyl$_2$(bdc)$_3$-DMOF-1** and **pbdc-5a-DMOF-1** show significantly lower decomposition temperatures (315 and 300 °C respectively), supporting the hypothesis that pentyl-tethered structures based on multiple repeating units show diminished stability (Fig. S57–S59†). We note that values for decomposition temperature are approximate due to the gradual slope of the mass loss steps, but provide helpful points of comparison between the materials in this study.

Scanning electron microscopy (SEM) conducted on selected tethered DMOFs reveals mixtures of discrete and intergrown crystals. Strikingly, the crystals of **pentyl(bdc)$_2$-DMOF-1** show a distinct hexagonal morphology (Fig. 8(a)). In contrast, **pentyl$_2$(bdc)$_3$-DMOF-1** forms cuboidal rod-like crystals (Fig. 8(b) and S60†), and **pbdc-5a-DMOF-1** forms tapered cuboidal crystals together with smaller, intergrown nanocrystals. **Heptyl(bdc)$_2$-DMOF-1** and ***m*-xylyl(bdc)$_2$-DMOF-1** form mixtures of cuboidal and irregular block-shaped crystals (Fig. 8(c) and S61†), and **pbdc-7a-DMOF** forms a mixture of aggregated needle crystals and larger cuboidal crystals (Fig. 8(d)). Therefore, the **kag** structure of **pentyl(bdc)$_2$-DMOF-1** results in the adoption of crystals with hexagonal symmetry, whereas the cross-linked **pcu** DMOFs adopt morphologies with square cross-sections. These morphologies are consistent with the layer structure in each set of materials and with the morphologies shown by crystals of the parent MOFs.[17,18] Unlike some previously reported polyMOFs, **pbdc-5a-DMOF-1** and **pbdc-7a-DMOF-1** do not show significant hierarchical structuring of individual crystallites.[46] While we cannot rule out the formation of amorphous polymer-only domains, the combination of FTIR, SEM, and digestion NMR data strongly suggests that such domains – implying larger fractions of uncoordinated carboxylate groups and ligand to dabco ratios than those observed – do not comprise more than *ca.* 10% of the final polyDMOF materials.

Observations from the various experiments detailed above can be rationalized from analysis of the parent **kag-** and **pcu-DMOF-1** structures. Both structures are based on pillared layers, with dinuclear Zn(II) paddlewheel SBUs providing their equatorial sites for layer formation through four ditopic bdc^{2-} ligands, and their axial sites for pillaring through neutral ditopic dabco ligands. The key difference between the structures is that the **pcu** network is constructed by the pillaring of **sql** sheets in which bdc^{2-} ligands make angles of *ca.* 90° with the paddlewheel axis, while the **kag** network consists of pillared **kgm** sheets in which bdc^{2-} ligands make angles of *ca.* 60° and *ca.* 120° with the paddlewheel axis (Fig. 9).

This results in structures that have approximately equal interlayer distances, governed by the size of the pillaring dabco ligand, but distinct pore architectures. **pcu-DMOF-1** has uniform channels with a square cross section bounded by four bdc^{2-} ligands. In contrast, **kag-DMOF-1** has two types of channels, one narrow and triangular, and the other wide and hexagonal. Considering that tethering groups are bound to ether substituents on the bdc^{2-} ligand, distances measured between aryl protons in the crystal structures of the parent frameworks provide an approximate measure of the space available for tether incorporation between pairs of bdc linkers. The interlayer distances in **pcu-DMOF-1** (7.5 Å) and **kag-DMOF-1** (7.4 Å) are very similar and do not provide a basis for structure directing effects upon tether incorporation. However, the distances between perpendicular (6.7 Å) and parallel (8.7 Å) pairs of bdc^{2-} ligands in **pcu-DMOF-1**, and the narrow triangular channel in **kag-DMOF-1** (5.9 Å) are in the appropriate range for the tethers studied here to exert an influence over framework formation.

Histograms were generated from the crystal structures deposited in the Cambridge Structural Database (CSD, see ESI for details†) of O···O distances between oxygen atoms bridged by alkyl and xylyl groups that are used as tethers in our study (Table S4 and Fig. S62†), to illustrate the typical range of distances shown by each tethering group in crystal structures.[47]

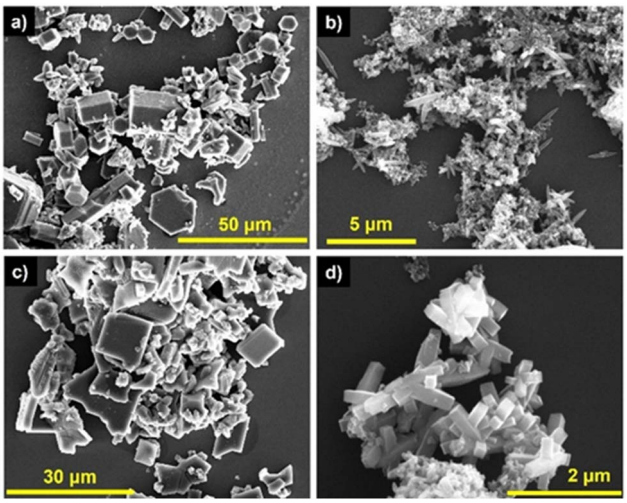

Fig. 8 Scanning Electron Microscopy (SEM) images of (a) pentyl(bdc)$_2$-DMOF-1, (b) pbdc-5a-DMOF-1, (c) heptyl(bdc)$_2$-DMOF-1, and (d) pbdc-7a-DMOF-1.

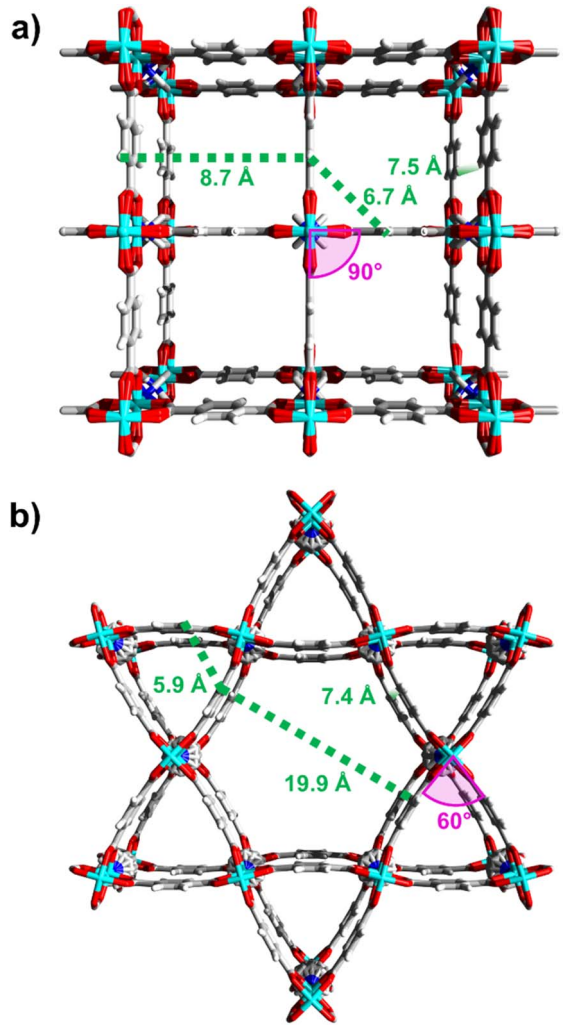

Fig. 9 Perspective views of the crystal structures of (a) **pcu-DMOF-1** and (b) **kag-DMOF-1**, with highlighted inter-ligand distances and angles.

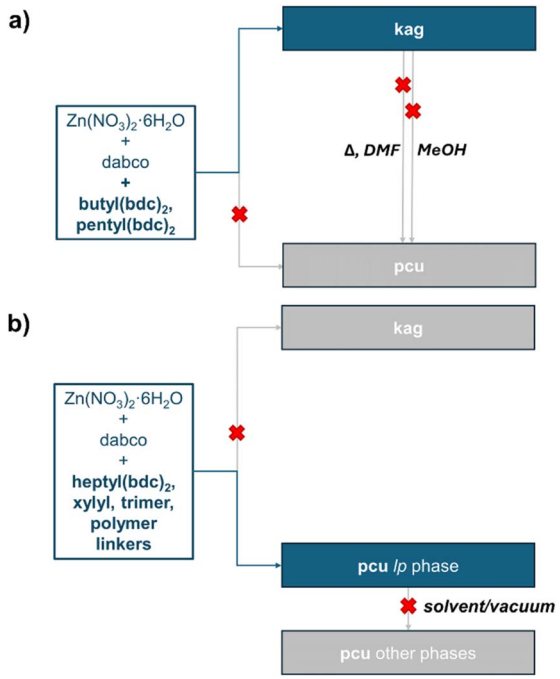

Fig. 10 Schematic representation of the DMOF phases accessible to (a) butyl- and pentyl-tethered dimeric bdc ligands; (b) heptyl-tethered dimeric, pentyl-tethered dimeric, and polymeric bdc ligands.

It was found that most butyl chains and a significant fraction of pentyl chains in reported structures adopt conformations resulting in O···O distance below the 5.9 Å value associated with the narrow pore in **kag-DMOF-1**. In contrast, histograms for the hexyl and heptyl tethers show distributions with no distances below 6.0 Å, which provides an empirical justification for the structure directing behavior observed. *m*-Xylyl and *p*-xylyl groups show distributions centered around *ca.* 6.5 Å and 7 Å respectively, compatible with the **pcu** structure they adopt. However, *o*-xylyl groups show distances only in the 4–6 Å range yet prefer the **pcu** structure. This suggests that additional factors such as tether rigidity play a role in structure selection. The narrow triangular pore in the **kag** structure may be accessible to the butyl tether of comparable length due to its flexibility and ability to contort into the confined space presented by the pore, while remaining inaccessible to the rigid *o*-xylyl tether.

Similar factors can explain the formation of the **kag** network by the dimeric pentyl-tethered ligand, and the **pcu** network by its trimeric and polymeric counterparts. Although the pentyl tether is short and flexible enough to bridge two bdc^{2-} groups in the triangular pore of the **kag** structure, any additional pentyl tether from the same bdc^{2-} unit would be required to traverse the hexagonal pore, in which parallel bdc^{2-} ligands are 19.9 Å apart, and adjacent ligands are 6.7 Å apart at a very obtuse angle. In these circumstances, we propose that the formation of a strained **pcu** structure becomes favored over **kag**, as seen in **pentyl$_2$(bdc)$_3$-DMOF-1** and **pbdc-5a-DMOF-1**. The modified relationships between phases and topologies upon tether incorporation are summarized in Fig. 10.

Conclusions

In this work, we have synthesized and characterized several new DMOFs based on oligomeric and polymeric linkers, with varying cross-link length, flexibility, and number of repeating ligand units. Our results show that although oligomeric and polymeric terephthalate-based ligands with dabco co-ligands adopt the canonical **pcu-DMOF-1** structure in most cases, the ultimate structures are dictated by the length and flexibility of the tethering group. Specifically, we find that butyl- and pentyl-tethered dimers adopt an isomeric **kag** structure even under thermodynamically forcing conditions, whereas more rigid xylyl tethers of comparable length, or longer heptyl tethers adopt the parent **pcu** structure. Upon linking three or more terephthalate groups using pentyl spacers, we have found that ligands become incompatible with the **kag** structure and revert to **pcu**. Therefore, oligoMOFs based on dimeric ligands can form distinct structures from those based on trimers, or the corresponding polyMOFs under identical conditions, depending on the

specific framework structure. These results are the first example of flexible inter-ligand tethers acting as structure-directing elements in MOFs and show that the influences of these tethers on overall structure are more nuanced than previously realized.

Furthermore, we have shown that the phase transformations shown by the parent **pcu-DMOF-1** are altered upon cross-link incorporation, and the large pore phase is stabilized. The solvent-mediated transformation of **kag-DMOF-1** to **pcu-DMOF-1** is also rendered inaccessible upon cross-link incorporation. Therefore, the phase and topological landscapes of the **kag-** and **pcu-DMOF-1** structures have been shown to be highly sensitive to manipulation of the constraints over ligand geometry imposed by means of cross-linking moieties. The use of hexyl-tethered dimeric ligands further resulted in the formation of a possible new isomeric phase of DMOFs, showing that cross-links may also provide a route to novel structures. Understanding the impact of ligand cross-links as design elements represents a step towards enhanced understanding of MOF-polymer compatibility.

Data availability

The data supporting this article have been included as part of the ESI.†

Author contributions

D. S. and S. M. C designed the materials and experimental strategy; D. S. conducted the experiments; D. S. and S. M. C wrote the manuscript. All authors have given approval to the final version of the manuscript.

Conflicts of interest

There are no conflicts to declare.

Acknowledgements

This work was supported by the Department of Energy, Office of Basic Energy Sciences, Division of Materials Science and Engineering (under Award No. DE-FG02-08ER46519). Preliminary funding was provided by the Defense Threat Reduction Agency (under Award No. HDTRA-12210037). We thank Dr Yongxuan Su for mass spectrometry at the Molecular Mass Spectrometry Facility at UC San Diego. We also thank Dr Minjung Kang for SEM images collected at the San Diego Nano-Technology Infrastructure (SDNI) of UC San Diego, a member of the National Nanotechnology Coordinated Infrastructure, which is supported by the National Science Foundation (ECCS-1542148). This work also made use of facilities and instrumentation at the UC San Diego Materials Research Science and Engineering Center (UCSD MRSEC, grant #DMR-2011924, supported by NSF), and the UC San Diego Department of Nanoengineering Materials Research Center (NE-MRC).

References

1 O. M. Yaghi, H. Li, C. Davis, D. Richardson and T. L. Groy, *Acc. Chem. Res.*, 1998, **31**, 474–484.
2 B. F. Hoskins and R. Robson, *J. Am. Chem. Soc.*, 1989, **111**, 5962–5964.
3 S. Kitagawa, R. Kitaura and S.-i. Noro, *Angew. Chem., Int. Ed.*, 2004, **43**, 2334–2375.
4 G. Férey, *J. Solid State Chem.*, 2000, **152**, 37–48.
5 B. Moulton and M. J. Zaworotko, *Chem. Rev.*, 2001, **101**, 1629–1658.
6 H. Furukawa, Y. B. Go, N. Ko, Y. K. Park, F. J. Uribe-Romo, J. Kim, M. O'Keeffe and O. M. Yaghi, *Inorg. Chem.*, 2011, **50**, 9147–9152.
7 H. Deng, S. Grunder, K. E. Cordova, C. Valente, H. Furukawa, M. Hmadeh, F. Gándara, A. C. Whalley, Z. Liu, S. Asahina, H. Kazumori, M. O'Keeffe, O. Terasaki, J. F. Stoddart and O. M. Yaghi, *Science*, 2012, **336**, 1018–1023.
8 M. Eddaoudi, J. Kim, N. Rosi, D. Vodak, J. Wachter, M. O'Keeffe and O. M. Yaghi, *Science*, 2002, **295**, 469–472.
9 R. Freund, S. Canossa, S. M. Cohen, W. Yan, H. Deng, V. Guillerm, M. Eddaoudi, D. G. Madden, D. Fairen-Jimenez, H. Lyu, L. K. Macreadie, Z. Ji. Y. Zhang, B. Wang, F. Haase, C. Woll, O. Zaremba, J. Andrea, S. Wuttke and C. S. Diercks, *Angew. Chem., Int. Ed.*, 2021, **60**, 23946–23974.
10 T. L. Hennigar, D. C. MacQuarrie, P. Losier, R. D. Rogers and M. J. Zaworotko, *Angew. Chem., Int. Ed.*, 1997, **36**, 972–973.
11 A. Karmakar, A. Paul and A. J. L. Pombeiro, *CrystEngComm*, 2017, **19**, 4666–4695.
12 N. Zhu, D. Sensharma, P. Wix, M. J. Lennox, T. Düren, W. Y. Wong and W. Schmitt, *Eur. J. Inorg. Chem.*, 2016, 1943–1947.
13 F. Carson, J. Su, A. E. Platero-Prats, W. Wan, Y. Yun, L. Samain and X. Zou, *Cryst. Growth Des.*, 2013, **13**, 5036–5044.
14 T. Tanasaro, K. Adpakpang, S. Ittisanronnachai, K. Faungnawakij, T. Butburee, S. Wannapaiboon, M. Ogawa and S. Bureekaew, *Cryst. Growth Des.*, 2018, **18**, 16–21.
15 M. Perfecto-Irigaray, G. Beobide, O. Castillo, I. da Silva, D. García-Lojo, A. Luque, A. Mendia and S. Pérez-Yáñez, *Chem. Commun.*, 2019, **55**, 5954–5957.
16 Y.-B. Zhang, H. Furukawa, N. Ko, W. Nie, H. J. Park, S. Okajima, K. E. Cordova, H. Deng, J. Kim and O. M. Yaghi, *J. Am. Chem. Soc.*, 2015, **137**, 2641–2650.
17 D. N. Dybtsev, H. Chun and K. Kim, *Angew. Chem., Int. Ed.*, 2004, **43**, 5033–5036.
18 H. Chun and J. Moon, *Inorg. Chem.*, 2007, **46**, 4371–4373.
19 M. Kondo, Y. Takashima, J. Seo, S. Kitagawa and S. Furukawa, *CrystEngComm*, 2010, **12**, 2350–2353.
20 K. Zhou, S. Chaemchuen, Z. Wu and F. Verpoort, *Microporous Mesoporous Mater.*, 2017, **239**, 28–33.
21 J. Hungerford and K. S. Walton, *Inorg. Chem.*, 2019, **58**, 7690–7697.

22 S. Chaemchuen, K. Zhou, M. S. Yusubov, P. S. Postnikov, N. Klomkliang and F. Verpoort, *Microporous Mesoporous Mater.*, 2019, **278**, 99–104.
23 S. Henke, R. Schmid, J. D. Grunwaldt and R. A. Fischer, *Chem. Eur. J.*, 2010, **16**, 14296–14306.
24 S. Henke, A. Schneemann, A. Wütscher and R. A. Fischer, *J. Am. Chem. Soc.*, 2012, **134**, 9464–9474.
25 A. Schneemann, S. Henke, I. Schwedler and R. A. Fischer, *ChemPhysChem*, 2014, **15**, 823–839.
26 L. K. Cadman, J. K. Bristow, N. E. Stubbs, D. Tiana, M. F. Mahon, A. Walsh and A. D. Burrows, *Dalton Trans.*, 2016, **45**, 4316–4326.
27 H. Hahm, K. Yoo, H. Ha and M. Kim, *Inorg. Chem.*, 2016, **55**, 7576–7581.
28 H. Ha, H. Hahm, D. G. Jwa, K. Yoo, M. H. Park, M. Yoon, Y. Kim and M. Kim, *CrystEngComm*, 2017, **19**, 5361–5368.
29 M. Kim, J. A. Boissonnault, P. V. Dau and S. M. Cohen, *Angew. Chem., Int. Ed.*, 2011, **51**, 12193–12196.
30 Z. Wang and S. M. Cohen, *J. Am. Chem. Soc.*, 2009, **131**, 16675–16677.
31 H. Kim and S. M. Cohen, *Inorg. Chem.*, 2024, **63**, 1853–1857.
32 R. A. Dodson, J. Park, J. Kim, M. J. Cliffe and S. M. Cohen, *Inorg. Chem.*, 2022, **61**, 12284–12292.
33 C. A. Allen, J. A. Boissonnault, J. Cirera, R. Gulland, F. Paesani and S. M. Cohen, *Chem. Commun.*, 2013, **49**, 3200–3202.
34 C. Allen and S. Cohen, *Inorg. Chem.*, 2014, **53**, 7014–7019.
35 Z. Zhang, H. T. H. Nguyen, S. A. Miller and S. M. Cohen, *Angew. Chem., Int. Ed.*, 2015, **54**, 6152–6157.
36 P. G. Mileo, S. Yuan, S. Ayala Jr, P. Duan, R. Semino, S. M. Cohen, K. Schmidt-Rohr and G. Maurin, *J. Am. Chem. Soc.*, 2020, **142**, 10863–10868.
37 D. S. Rollins, J. Geary, A. H. Wong and D. J. Xiao, *Chem. Commun.*, 2022, **58**, 12361–12364.
38 J. Geary, J. P. Aalto and D. J. Xiao, *Chem. Mater.*, 2024, **36**, 3949–3956.
39 Y. Gu, M. Huang, W. Zhang, M. A. Pearson and J. A. Johnson, *Angew. Chem., Int. Ed.*, 2019, **58**, 16676–16681.
40 M. MacLeod and J. Johnson, *Polym. Chem.*, 2017, **8**, 4488–4493.
41 J. Jiao, H. Liu, D. Bai and Y. He, *Inorg. Chem.*, 2016, **55**, 3974–3979.
42 L. Feng, K.-Y. Wang, X.-L. Lv, J. A. Powell, T.-H. Yan, J. Willman and H.-C. Zhou, *J. Am. Chem. Soc.*, 2019, **141**, 14524–14529.
43 J. Geary, A. H. Wong and D. J. Xiao, *J. Am. Chem. Soc.*, 2021, **143**, 10317–10323.
44 S. Ayala, K. C. Bentz and S. M. Cohen, *Chem. Sci.*, 2019, **10**, 1746–1753.
45 Z. Zhang, H. T. H. Nguyen, S. A. Miller, A. M. Ploskonka, J. B. DeCoste and S. M. Cohen, *J. Am. Chem. Soc.*, 2016, **138**, 920–925.
46 S. Ayala, Z. Zhang and S. M. Cohen, *Chem. Commun.*, 2017, **53**, 3058–3061.
47 C. R. Groom, I. J. Bruno, M. P. Lightfoot and S. C. Ward, *Acta Crystallogr., Sect. B: Struct. Sci., Cryst. Eng. Mater.*, 2016, **72**, 171–179.